Supplementary Information

Effects of aggregate size distribution and carbon nanotubes on mechanical properties of cemented gangue backfill samples under true triaxial compression

Qian Yin[1,2)], *Fan Wen*[1),✉], *Zhigang Tao*[3)], *Hai Pu*[1,4)], *Tianci Deng*[1)], *Yaoyao Meng*[2)], *Qingbin Meng*[1)], *Hongwen Jing*[1)], *Bo Meng*[1)], and *Jiangyu Wu*[1),✉]

1) State Key Laboratory of Intelligent Construction and Healthy Operation and Maintenance of Deep Underground Engineering, China University of Mining and Technology, Xuzhou 221116, China

2) State Key Laboratory of Mining Response and Disaster Prevention and Control in Deep Coal Mines, Anhui University Of Science and Technology, Huainan 232001, China

3) State Key Laboratory for Geomechanics & Deep Underground Engineering, China University of Mining and Technology (Beijing), Beijing 100083, China

4) Key Laboratory of Xinjiang Coal Resources Green Mining, Ministry of Education, Xinjiang Institute of Engineering, Urumqi 830023, China

✉ Corresponding authors: Fan Wen E-mail: w15135313372@163.com;

Jiangyu Wu E-mail: wujiangyu@cumt.edu.cn

The parameters of each material:

In this study, the gangue was sourced from the Xin'an Coal Mine in Shandong Province, China, and the mechanical parameters are presented in Table S1, where UCS represents uniaxial compressive strength, BTS represents Brazilian tensile strength, and E represents elastic modulus. CNTs were employed as an auxiliary additive to cement to improve the mechanical properties of the cementitious materials, and the main performance parameters are detailed in Table S2.

Table S1. Mechanical parameters of gangue

Density (g/cm^3)	UCS (MPa)	BTS (MPa)	*E* (GPa)
2.82	25.32	2.64	3.03

Table S2. Performance parameters of MWCNTs

Product name	Fineness (wt%)	Inside diameter (nm)	Outside diameter (nm)	Specific surface area (m^2/g)	Actual density (g/cm^3)
HQNANO-CNTs-010	>95	3–5	8–15	>233	2.1

Preparation of CGBSs:

A WH1200B ultrasonicator was used for the ultrasonic dispersion of CNTs, as shown in Fig. S1(a). Based on previous research [1], the ultrasonication time and power were set at 10 min and 150 W. The entire process was conducted in an ice-water mixture to prevent the generation of heat during ultrasonication from affecting the properties of the CNTs. The CNT suspensions were prepared at P_{CNT} = 0, 0.04%, 0.08%, and 0.12%, respectively. The required quantities of CNT powder and water were accurately weighted by an analytical balance with a precision of 0.001 g. The CNT powder was then introduced into the water, thoroughly mixed with a glass rod, and subjected to ultrasonic dispersion to achieve CNT suspensions. The mass ratio of fly ash to cement was set at 1:4, with a water-to-cement ratio of 0.75 [2]. The information of material proportion is listed in Table S3. A predetermined amount of fly ash and cement was mixed for 3 min using a mixer in the dry state before the addition of the prepared CNT suspensions. The homogenous CNT cement paste was prepared after thorough mixing.

Table S3. Material proportions

P_{CNT} (wt%)	D	Mass ratio of fly ash to cement	Mass ratio of slurry to aggregate	Mass ratio of water to (fly ash + cement)
0.00	2.150	1:4	3:5	3:4
0.00	2.325	1:4	3:5	3:4
0.00	2.500	1:4	3:5	3:4
0.00	2.675	1:4	3:5	3:4
0.00	2.850	1:4	3:5	3:4
0.04	2.150	1:4	3:5	3:4
0.04	2.325	1:4	3:5	3:4
0.04	2.500	1:4	3:5	3:4
0.04	2.675	1:4	3:5	3:4
0.04	2.850	1:4	3:5	3:4
0.08	2.150	1:4	3:5	3:4
0.08	2.325	1:4	3:5	3:4
0.08	2.500	1:4	3:5	3:4
0.08	2.675	1:4	3:5	3:4
0.08	2.850	1:4	3:5	3:4
0.12	2.150	1:4	3:5	3:4
0.12	2.325	1:4	3:5	3:4
0.12	2.500	1:4	3:5	3:4
0.12	2.675	1:4	3:5	3:4
0.12	2.850	1:4	3:5	3:4

The aggregate particle size distribution equation for fractal theory is derived as follows [3]:

For aggregates with particle size d, number N, and mass M, the particle size distribution (PSD) equation and mass distribution equation are Eq. (1) and Eq. (2) respectively.

$$F(d) = \frac{N}{N_t} \tag{1}$$

$$P(d) = \frac{M}{M_t} \tag{2}$$

where N_t is the total number of aggregate particles, M is the mass of aggregate with particle size less than d, and M_t is the total mass of aggregates.

The following relationship exists between the number of aggregate particles and aggregate size:

$$N = C_0 + C_1\left(\frac{d}{d_{max}}\right)^{-D} \tag{3}$$

where D is the fractal dimension of aggregate particle size distribution, d_{max} is the maximum particle size of aggregate particles, C_0 and C_1 are the parameters related to fractal distribution.

There are two boundary conditions in the above equation, namely $F(d_{max}) = 1$ and $F(d_{min}) = 0$. Thus, Eq. (4) is derived:

$$F(d) = \frac{d^{-D} - d_{min}^{-D}}{d_{max}^{-D} - d_{min}^{-D}} \tag{4}$$

where d_{min} is the minimum particle size of aggregate particles.

The following relationship exists between the number of aggregate particles and aggregate size:

$$M = V\rho N \tag{5}$$

$$V \propto kd^3 \tag{6}$$

where V is the volume of aggregate particles of particle size d, ρ is the density of aggregate particles, and k is a parameter related to the volume shape.

Eqs. (1)–(6) are joined to differentiate and integrate, and the aggregate particle size distribution equation based on fractal theory is obtained, as shown in Eq. (7):

$$Q_i = \frac{M_i}{M_t} = \frac{d_i^{3-D} - d_{min}^{3-D}}{d_{max}^{3-D} - d_{min}^{3-D}} \tag{7}$$

where d_i represents the aperture of each grading sieve, d_{min} represents the minimum aperture of the grading scree, d_{max} denotes the maximum aperture of the grading screen, M_i is the mass of the aggregate with a size in the d_i–d_{min} zone, M_t represents the total mass of the aggregates, and Q_i denotes the interval particle size distribution mass fraction.

Each CGBS had a total aggregate mass of 400 g. According to Eq. (7), specific parameters of aggregate mass distribution for a single specimen can be calculated in Table S4.

Table S4. Aggregate mass distribution for a single specimen

	Mass of aggregate particles in each size interval (g)							
D	0.25–1.0 mm	1.0–1.5 mm	1.5–2.5 mm	2.5–4 mm	4–6 mm	6–8 mm	8–10 mm	Total (g)
2.150	56.50	23.25	43.36	60.46	75.54	71.78	69.11	400
2.325	84.54	26.61	45.76	58.58	67.84	60.73	55.93	400
2.500	126.49	28.43	45.08	52.98	56.86	47.93	42.23	400
2.675	189.26	26.66	38.99	42.07	41.83	33.21	27.98	400
2.850	283.18	17.76	23.97	23.73	21.86	16.34	13.17	400

The prepared CNT cement paste was mixed with the uniformly stirred aggregates for 8 minutes before being poured into customized acrylic molds with dimensions 50 mm × 70 mm × 100 mm. By low-speed vibration, until no bubbles were generated on the surface of the CGBSs, the sample was left to stand for 24 hours and demolded. The CGBSs were placed in water and cured at room temperature for 28 days [4]. Finally, a high-precision cutting machine was used to cut the CGBSs to

obtain rectangular samples of 50 mm × 50 mm × 100 mm, ensuring a cross-sectional flatness of ± 0.02 mm (Fig. S1).

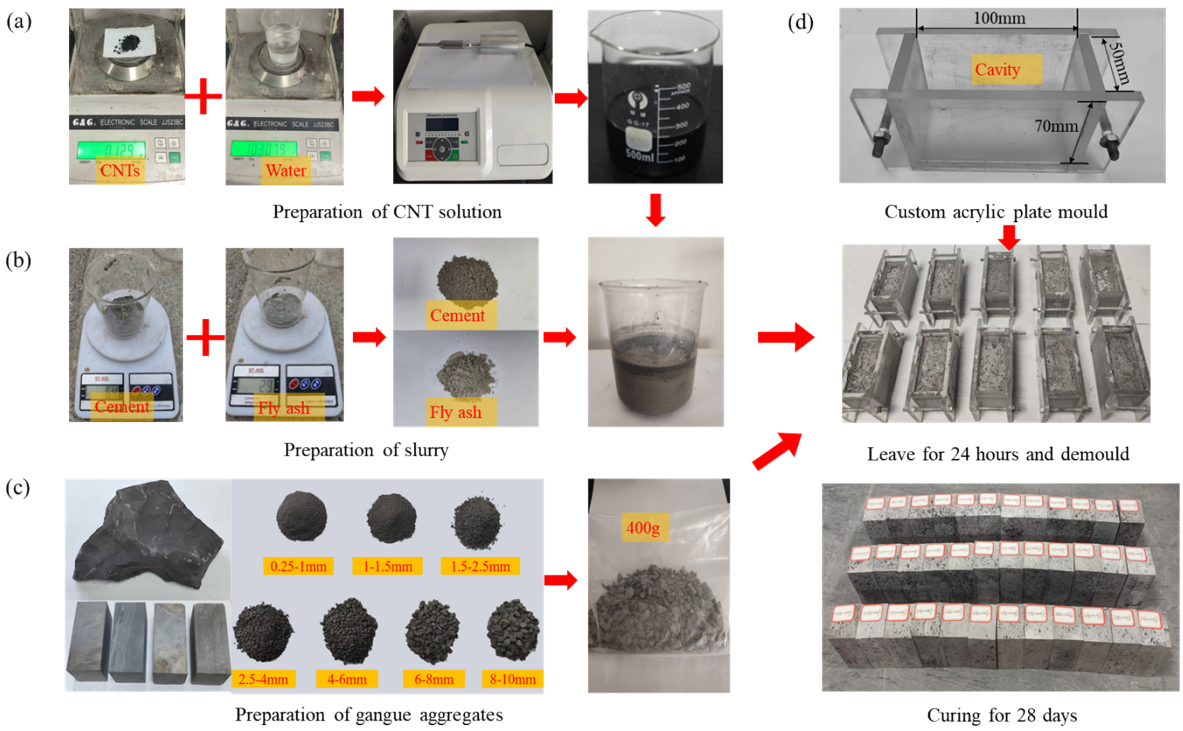

Fig. S1. Production process of CGBSs.

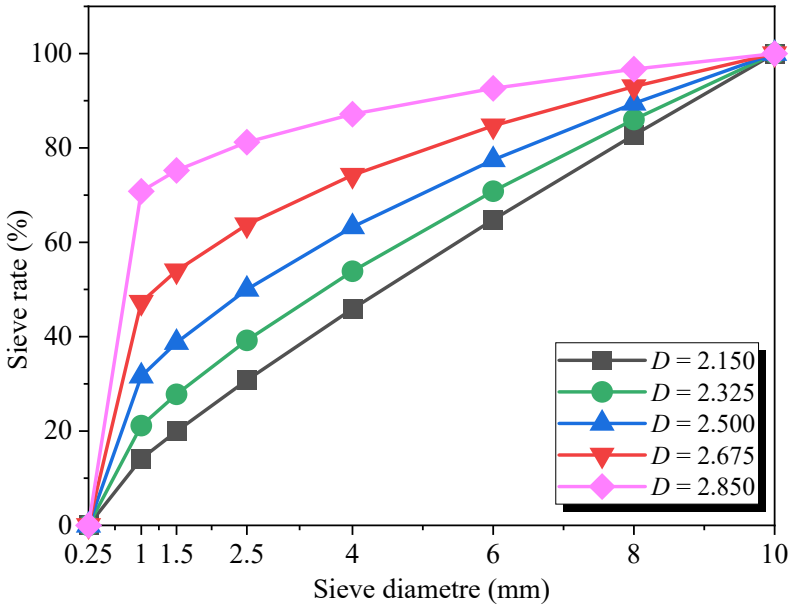

Fig. S2. Gradation curves of CGBSs with different *D*.

The testing instruments and steps are as follows:

True triaxial compression tests were conducted on CGBSs using a true triaxial electro-hydraulic servo loading test system, as shown in Fig. S3. The loading schemes are divided into three stages, and the loading path is illustrated in Fig. S4.

1) By a force-controlled loading method, the CGBSs were loaded to a hydrostatic pressure state at a loading rate of 0.1 MPa/s, until large principal stress (σ_1), medium principal stress (σ_2), and small principal stress (σ_3) were 5 MPa.

2) With σ_3 kept constant at 5 MPa, the loading rate was maintained to increase σ_1 and σ_2 until σ_2 = 10 MPa, thereby completing the application of lateral stress.

3) While keeping σ_2 and σ_3 unchanged, σ_1 was applied to the CGBSs at a displacement-controlled loading rate of 0.002 mm/s until the CGBSs failed.

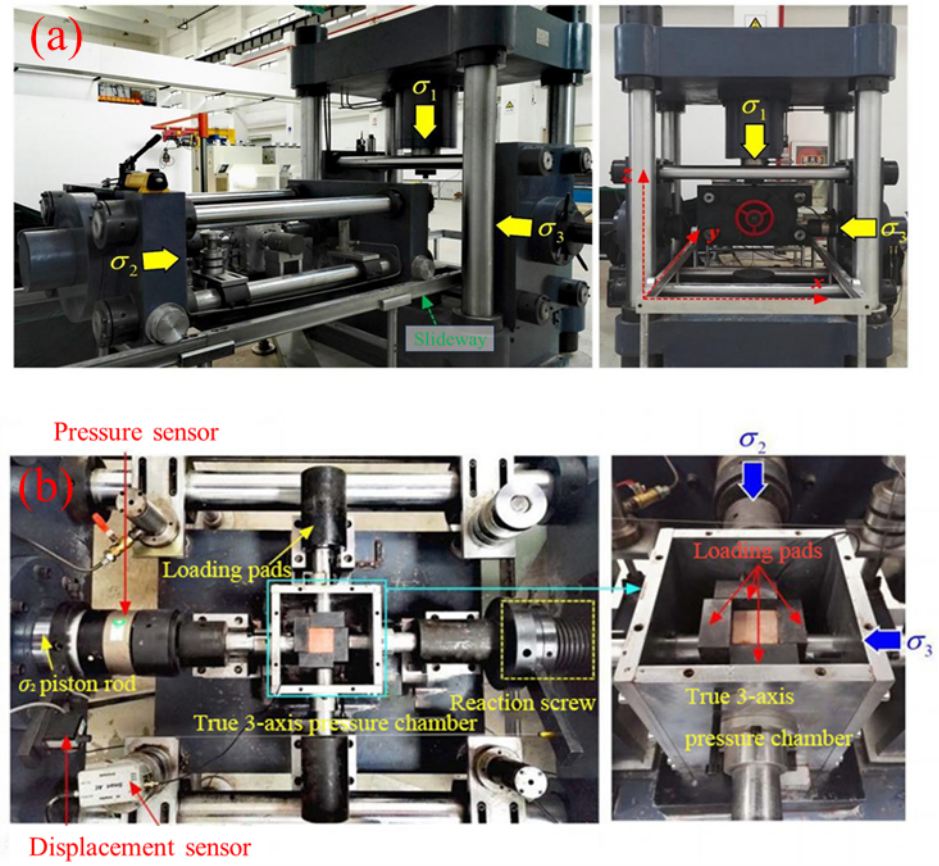

Fig. S3. True triaxial compression test system: (a) overall layout; (b) internal structure.

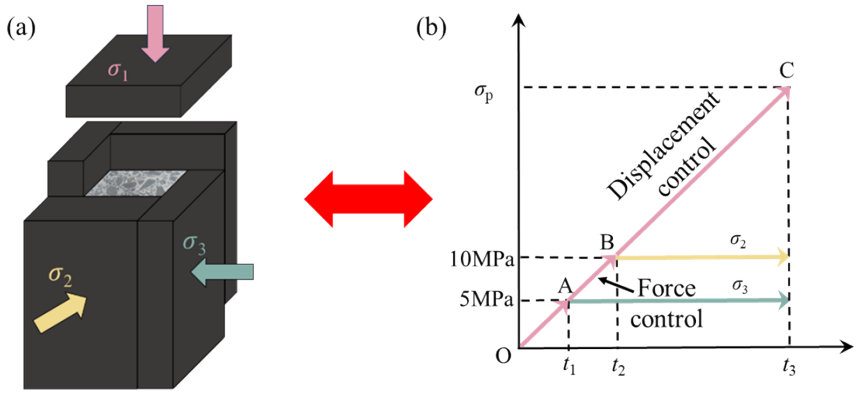

Fig. S4. True triaxial loading test program: (a) loading model; (b) loading path.

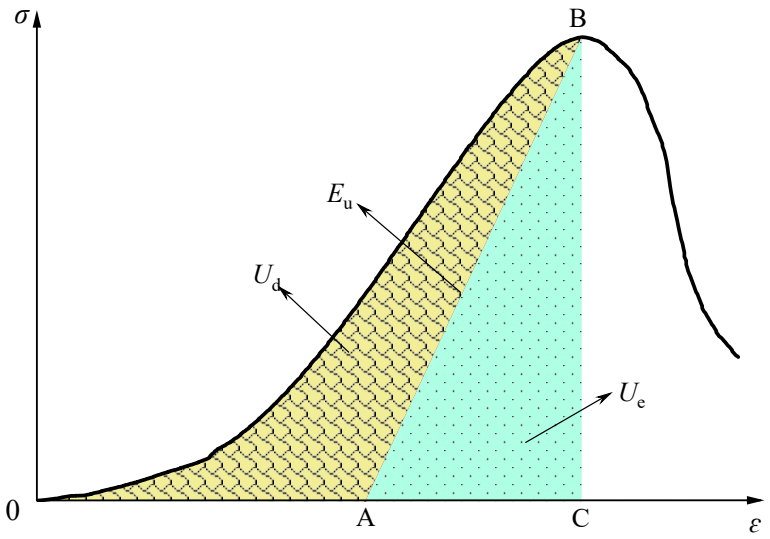

Fig. S5. Relationship between dissipation energy (U_d) and elastic strain energy (U_e).

Table S5. Energy parameters of CGBSs with different P_{CNT} when D = 2.500 at σ_p

D	P_{CNT} (wt%)	U (J/cm^3)	U_e (J/cm^3)	U_d (J/cm^3)	Proportion of U_e	Proportion of U_d
2.500	0.00	0.92	0.39	0.53	0.42	0.58
	0.04	1.24	0.43	0.81	0.35	0.65
	0.08	1.46	0.46	1.00	0.31	0.69
	0.12	1.01	0.41	0.60	0.41	0.59

Table S6. Energy parameters of CGBSs with different D when P_{CNT} = 0.08wt% at σ_p

P_{CNT} (wt%)	D	U (J/cm^3)	U_e (J/cm^3)	U_d (J/cm^3)	Proportion of U_e	Proportion of U_d
0.08	2.150	1.36	0.50	0.86	0.37	0.63
	2.325	1.39	0.48	0.91	0.35	0.65
	2.500	1.46	0.46	1.00	0.31	0.69
	2.675	1.19	0.32	0.87	0.27	0.73
	2.850	1.00	0.24	0.76	0.25	0.75

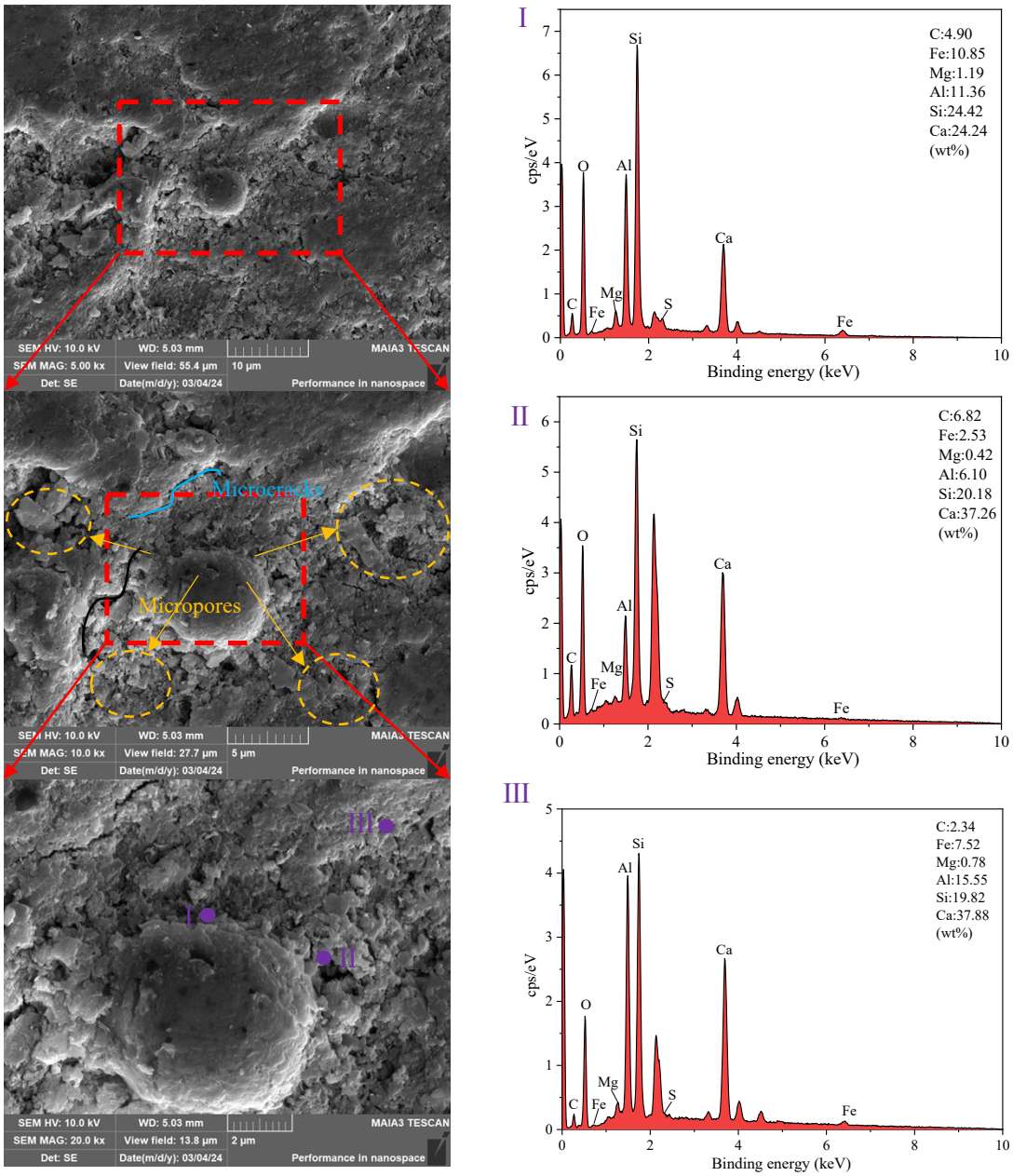
SEM HV: 10.0 kV
WD: 5.03 mm
MAIA3 TESCAN
SEM MAG: 5.00 kx
View field: 55.4 μm
10 μm
Det: SE
Date(m/d/y): 03/04/24
Performance in nanospace
Microcracks
Micropores
SEM HV: 10.0 kV
WD: 5.03 mm
MAIA3 TESCAN
SEM MAG: 10.0 kx
View field: 27.7 μm
5 μm
Det: SE
Date(m/d/y): 03/04/24
Performance in nanospace
III
I
II
SEM HV: 10.0 kV
WD: 5.03 mm
MAIA3 TESCAN
SEM MAG: 20.0 kx
View field: 13.8 μm
2 μm
Det: SE
Date(m/d/y): 03/04/24
Performance in nanospace
I
C:4.90
Fe:10.85
Mg:1.19
Al:11.36
Si:24.42
Ca:24.24
(wt%)
cps/eV
Binding energy (keV)
II
C:6.82
Fe:2.53
Mg:0.42
Al:6.10
Si:20.18
Ca:37.26
(wt%)
cps/eV
Binding energy (keV)
III
C:2.34
Fe:7.52
Mg:0.78
Al:15.55
Si:19.82
Ca:37.88
(wt%)
cps/eV
Binding energy (keV)

(a) $P_{CNT} = 0$

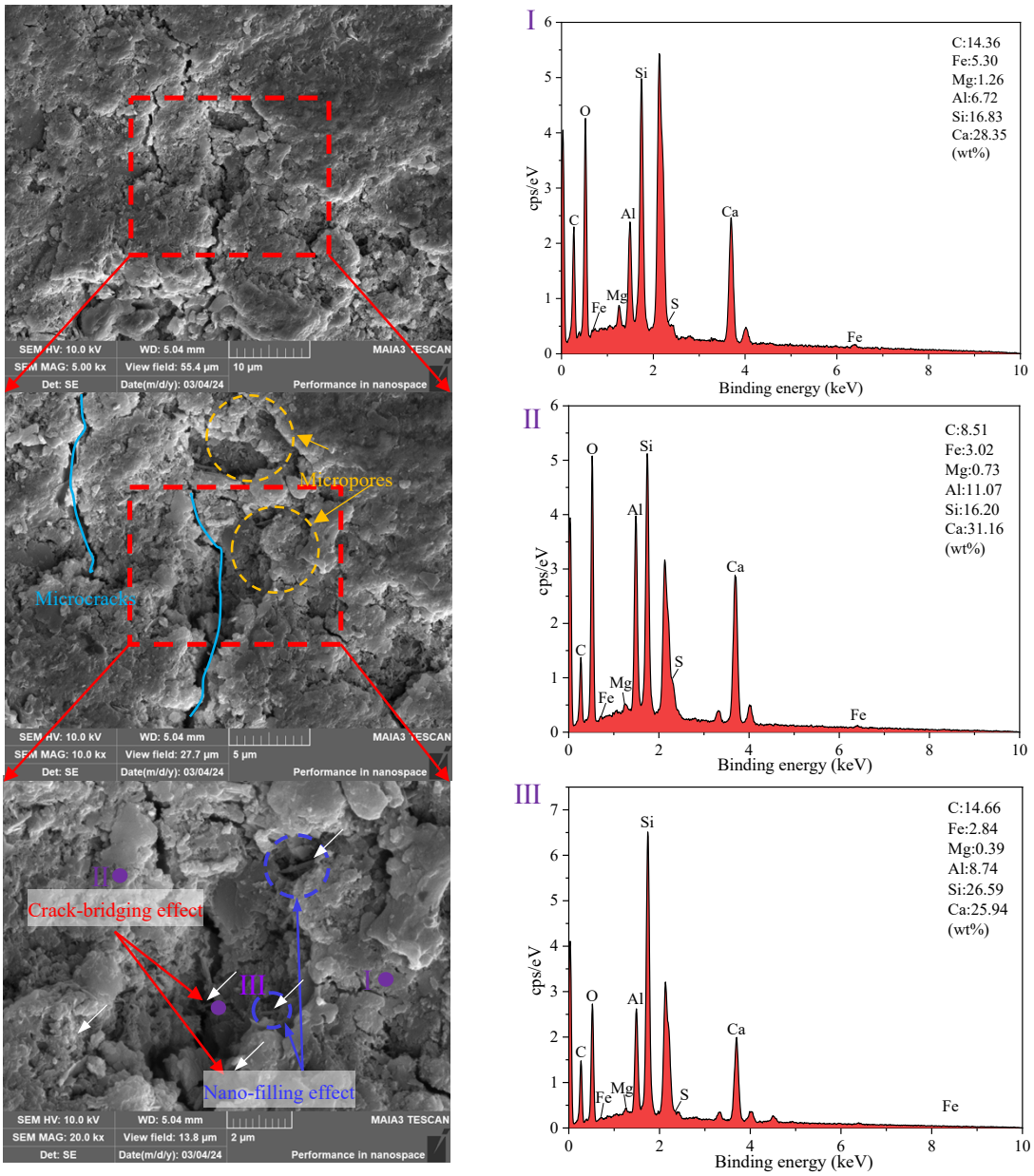
SEM HV: 10.0 kV
WD: 5.04 mm
MAIA3 TESCAN
SEM MAG: 5.00 kx
View field: 55.4 μm
10 μm
Det: SE
Date(m/d/y): 03/04/24
Performance in nanospace
Micropores
Microcracks
SEM HV: 10.0 kV
WD: 5.04 mm
MAIA3 TESCAN
SEM MAG: 10.0 kx
View field: 27.7 μm
5 μm
Det: SE
Date(m/d/y): 03/04/24
Performance in nanospace
II
Crack-bridging effect
III
I
Nano-filling effect
SEM HV: 10.0 kV
WD: 5.04 mm
MAIA3 TESCAN
SEM MAG: 20.0 kx
View field: 13.8 μm
2 μm
Det: SE
Date(m/d/y): 03/04/24
Performance in nanospace
I
C:14.36
Fe:5.30
Mg:1.26
Al:6.72
Si:16.83
Ca:28.35
(wt%)
cps/eV
Binding energy (keV)
II
C:8.51
Fe:3.02
Mg:0.73
Al:11.07
Si:16.20
Ca:31.16
(wt%)
cps/eV
Binding energy (keV)
III
C:14.66
Fe:2.84
Mg:0.39
Al:8.74
Si:26.59
Ca:25.94
(wt%)
cps/eV
Binding energy (keV)

(b) P_{CNT} = 0.04wt%

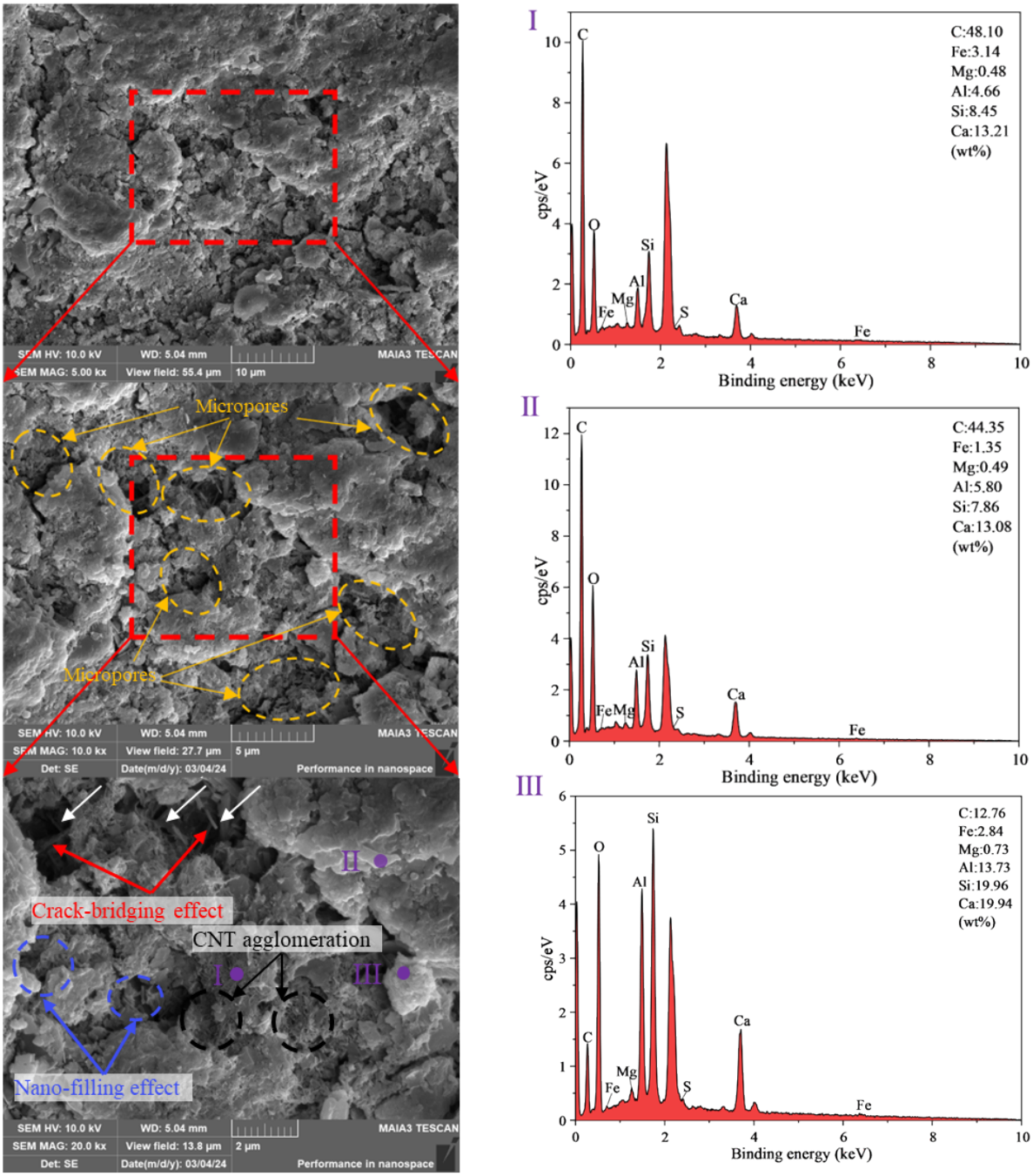

(c) P_{CNT} = 0.12%

Fig. S6. Microstructure of CGBSs with different P_{CNT} at D of 2.5: (a) P_{CNT} = 0; (b) P_{CNT} = 0.04wt%; (c) P_{CNT} = 0.12wt%.

.

References

[1] Y. Gao, H.W. Jing, S.J. Chen, M.R. Du, W.Q. Chen, and W.H. Duan, Influence of ultrasonication on the dispersion and enhancing effect of graphene oxide–carbon nanotube hybrid nanoreinforcement in cementitious composite, *Compos. B. Eng*., 164(2019), p. 45.

[2] J.P. Zuo, Z.J. Hong, Z.Q. Xiong, C. Wang, and H.Q. Song, Influence of different W/C on the performances and hydration progress of dual liquid high water backfilling material, *Constr. Build. Mater*., 190(2018), p. 910.

[3] J.Y. Wu, H.W. Jing, Y. Gao, Q. Meng, Q. Yin, and Y. Du, Effects of carbon nanotube dosage and aggregate size distribution on mechanical property and microstructure of cemented rockfill, *Cem. Concr. Compos*., 127(2022), art. No 104408.

[4] M. Fall, J.C. Célestin, M. Pokharel, and M. Touré contribution to understanding the effects of curing temperature on the mechanical properties of mine cemented tailings backfill, *Eng. Geol.*, 114(2010), No.3, p. 397.